

FORECASTING EXTRATROPICAL TRANSITION OF TROPICAL CYCLONE INTENSIFICATION VIA PROJECTION PURSUIT

3A.3

Oguz Demirci*

University of New Mexico, Albuquerque, New Mexico 87131

1. Introduction

As Tropical Cyclones (TC's) move poleward out of the tropics toward the midlatitudes, they move into a region of colder temperatures and associated higher wind shear. The interaction between the TC and an increasingly baroclinic regime is referred to as Extratropical Transition (ET). As the TC moves into the increasing baroclinic environment, it weakens, as measured by a rising central sea-level pressure. If it interacts favorably with midlatitude upper-level trough then it can reintensify as an extratropical cyclone or it eventually dissipates. Because ET is a highly variable process, the end result of this transition, either dissipation or intensification, is very hard to predict even with full physics capable systems (Jones et al. (2003)). Recent research by Ritchie and Elsberry (2005) has indicated that the outcome of the transition depends on the midlatitude pattern that the TC moves in, and the phasing between the TC and midlatitude upper-level troughs embedded within the large-scale midlatitude circulation. Figures 1 and 2 show Typhoon (TY) Peter (1997) and Supertyphoon (STY) Ivan (1997) with two different outcomes, intensification and dissipation, respectively. The analysis fields are from the U.S. Navy's Operational Global Atmospheric Prediction System (NOGAPS).

Harr et al. (2000) used Empirical Orthogonal Function (EOF) analysis to capture the spatial variation in 500-mb geopotential height analyses from NOGAPS. EOF analysis is a technique that can be used to reduce the dimensionality of a data set without compromising the explained variance among data classes. Harr et al. (2000) classified ET cases into two characteristic circulation patterns, northeast and northwest, based on the technique. Singular Value Decomposition (SVD) is a similar technique that can be used on two different fields to isolate coupled

modes of variability. Leuliette and Wahr (1999), Wallace et al. (1992) and Bretherton et al. (1992) used SVD as a coupled pattern analysis technique on sea surface temperature and sea surface height variables to explain the covariance between the two fields. Both EOF and SVD analyses are Projection Pursuit (PP) applications. Projection Pursuit is defined as the projection or projections from high to lower dimensional space by numerically maximizing a certain objective function called the projection index (Huber (1985)). PP algorithms are thus very useful as they reduce the dimensionality of the original observation space, usually by linear and/or nonlinear mapping or projection strategies.

Because Harr et al. (2000) found 500-mb analyses to be good indicators of different ET patterns, we also use them to capture the variability information both in the midlatitude upper-level troughs and TCs. We propose an algorithm composed of PP stages to predict whether an extratropical transitioning TC will reintensify or dissipate. We present two different methods involving multistage PP algorithms to identify the differences between intensifying and dissipating storms before ET time. We either combine the results obtained at spatial analysis at individual times (spatial technique) or combine the data from different times to take advantage of the variability information in time (spatiotemporal technique).

In the paper, we first describe the data in Section 2, and then characterize dimensionality reduction steps of the technique in Section 3. In Section 4, we present the results of the forecasting tool proposed at individual times, and spatiotemporal results are shown in Section 5. We conclude mentioning future plans in Section 6.

2. Data and Definitions

We used 12-h 500-mb geopotential height analyses from the Navy Operational Global Assimilation

* Corresponding author address: Oguz Demirci, Electrical and Computer Engineering Department, University of New Mexico, Albuquerque, NM 87131; e-mail: demirci@ece.unm.edu

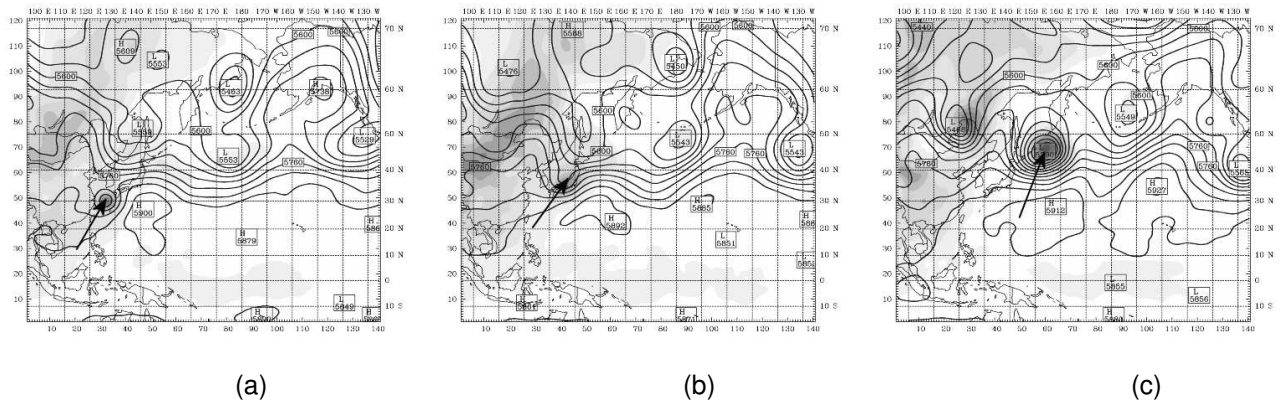


Figure 1: Positive Case (Peter 1997) in Northwestern Pacific: 500-mb Equipotential Height Analyses from NOGAPS for Typhoon Peter in 1997 at (a) June 27, 12Z, before ET (b) June 28, 12Z, at ET (c) and June 30, 00Z, after ET. Arrows indicate the location of the TC remnants

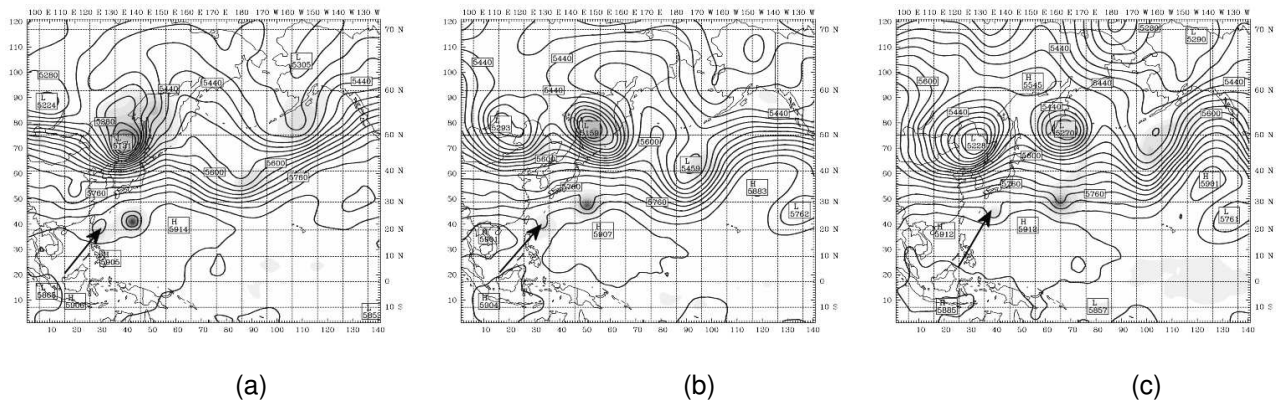


Figure 2: Null Case (Ivan 1997) in Northwestern Pacific: 500-mb Equipotential Height Analyses from NOGAPS for Super Typhoon Ivan in 1997 at (a) October 21, 00Z, before ET (b) October 22, 12Z, at ET (c) and October 24, 00Z, after ET. Arrows indicate the location of the TC remnants

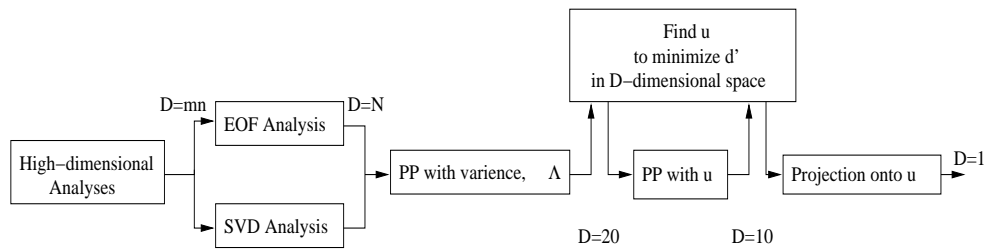


Figure 3: Organization of the classifier with Eigenanalysis and Projection Pursuit stages.

and Prediction System (NOGAPS). A total of 85 TCs underwent ET in the western North Pacific during 1997-2004. After removing missing data, 80 cases were retained for the study. The training set compared 53 storms from years 1997-2002, and 27 storms from years 2003-2004 constituted the test set. A common time (called ET+00h or the transition time) was determined for each TC as the first time that the TC first appears as an open wave in the 500-mb trough. This time is very close to the end of stage 1 of extratropical as defined by Klein et al. (2000). The NOGAPS analyses were interpolated to a 61° longitude \times 51° latitude grid at 1° resolution centered on the TC location starting 48-h prior to the ET+00h time to 48-h afterwards. This interval was chosen in order to ensure that the time interval covered the time when the storm was still a TC until well after the time of reintensification in positive cases. The TC location was determined using the Joint Typhoon Warning Center (JTWC) best track data when it was available and by examining the sea-level pressure data from the NOGAPS analysis when it was not. Sensitivity to domain was tested by reducing the resolution to 2° and trimming the domain, and this caused no significant change in performance.

For the purpose of this study, the storms were classified as either positive or negative cases using the minimum central pressure trace during ET from the NOGAPS analyses. If the sea-level pressure (SLP) of the storm decreased by more than 3 mb after the ET+00h time, it was called positive. Storms whose SLP values did not meet this criterion were classed as negative storms.

3. Analysis

The steps included in the classifier algorithm are summarized in Figure 3. Each step of the algorithm involves a reduction in the dimensionality of the original data set. A single NOGAPS 500-mb analysis, for the purposes of our study, contains $61 \times 51 = 3111$ points. Our training set comprises 53 cases of ET. Thus, each time of our analysis (9 in all, every 12-h from ET-48h to ET+48h) there are 53×3111 data points. This is considered a high-dimensional data set. Thus, we put the the data through a series of projection pursuit algorithms to reduce the dimensionality while retaining the information in the data that discriminates positive from negative cases.

The first step in the algorithm is an EOF analysis (Demirci et al. (2004)) that was applied to the training set every 12 hours from ET-48h to ET+48h. The output of the EOF analysis is a decomposition into

53 Principle Components (PCs) and their associated 61×51 dimensional EOFs.

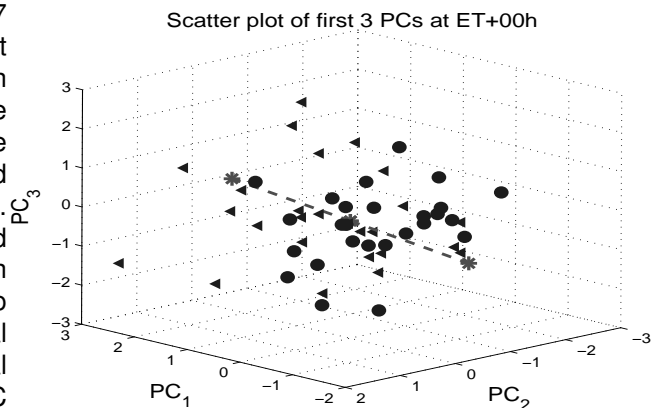


Figure 4: Distribution of the 53 storms in 1997-2002 in a 3D scatter plot at ET+00h. Positive storms are represented with circles and negative storms are represented with triangles. The coordinates of points are PCs. Maximum separation direction, \hat{u} , is represented with the line. The two ends and middle of the line are indicated with *.

The next step is to observe each storm in "PC-space". The storms are represented with the first three PC's in Figure 4 for visualization purposes only. The PCs are ordered by the amount of variance they represent in the original data set with PC1 explaining the largest portion ($> 50\%$). The first 20 PCs explain over 98% of the variance and are retained with all higher-order PCs being thrown out. As higher-order PCs tend to result in over-fitting of the data, this step serves to increase the stability of our system as well as decreasing the processing time and computational load. This reduces our original 61×51 dimensional data set first to 53-D and then 20-D.

Next, an *optimization* step is used to find the direction, \hat{u} , that maximized the separation of the positive and negative storm distributions. Various directions in 20-D PC space are examined and PCs of each storm are projected on each direction with a dot product operation. The details of the optimization step to find the \hat{u} direction in D-dimensional space are explained by Demirci et al. (2006). The 10 PCs, which carried more information in terms of separation, among the first 20 are then selected considering the \hat{u} direction found in the previous optimization step. Next, the same optimization step is repeated in the new 10 dimensional space and another \hat{u} direction maximizing the separation of two storm distributions is found. The storm coordinates are projected onto this \hat{u} direction found and each of the storm observations is represented with a projection distance value.

In order to use this method as a prediction tool, signal detection theory is used to decide whether a forecast storm belongs to the positive or the negative distributions, Poor (1994). The investigated storm is projected onto \hat{u} direction in the same fashion and a threshold value or minimum level of certainty has been used. We can then compute Detection rate (P_D) (i.e., probability of deciding that storm is an positive one when it really comes from the positive storm distribution), and a False Alarm rate (P_{FA}) (i.e., probability deciding that storm is a positive when it actually comes from the negative storm distribution). Estimates of each of these two probabilities can be computed and used to separate sensitivity from response bias. The Receiver Operating Characteristic (ROC) curve for the training data in Figure 6 shows the relationship between P_D and P_{FA} for all possible threshold values for the specific distribution in Figure 5.

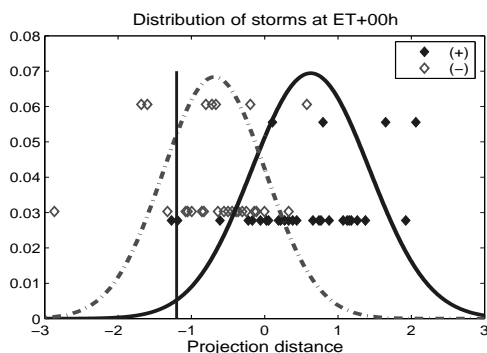


Figure 5: Histogram of positive and negative storm projection distances on maximum separation line at ET+00h. Positive storm frequencies were represented by filled diamonds and negatives by open diamonds. The distributions were represented by Gaussians. Vertical line shows a possible threshold.

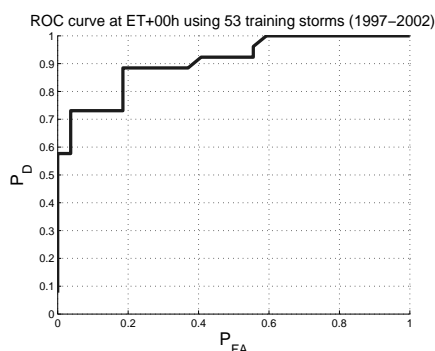


Figure 6: ROC curve obtained at ET+00h

The algorithm was applied to the data every 12 hours. The improvement in the training data ROC curves with time is summarized in Figure 7. We find that the separation distance and detection rates get better with time as the two distributions separate. The separation index, d' , increases rapidly with time

beginning at time ET-24h until ET+48h. Although the performance before ET and after ET differ significantly, rapid increase in d' before ET+00h is a promising sign that the classification can be successfully done before ET. At ET-12h, a P_D of 80% is obtained with P_{FA} of 25% using a training set of storms from 1997-2002. The same prediction rate is achieved with P_{FA} of 15% with NOGAPS.

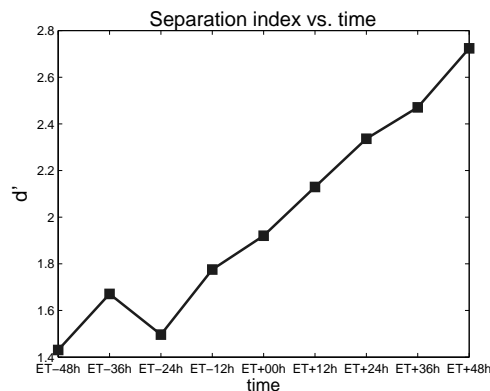


Figure 7: Separation index with time

4. Forecasting Tool

The real purpose of our research is developing a forecasting tool that predicts prior to ET+00h whether a storm is a positive or a negative ET case. To do this, we project our forecast storm onto the training data and objectively decide whether it is positive or negative based on where it falls. A forecast test was run using 27 Northwestern Pacific ET cases from 2003-2004 using the 53 cases from 1997-2002 as a training set.

The predicted false alarm rates of 10%, 20%, 30% and 40% have been calculated using the Gaussian distributions (e.g. Figure 5) and the results obtained for times ET-24h, ET-12h, ET+00h and ET+12h for 2003-2004 storms are tabulated in Table 1. Performance was poor for times earlier than ET-24h, and for times after ET+12h intensification is occurring for positive cases. The positive storms are indicated with gray rows. The True-False predictions for each case are represented with 1 and 0, respectively. The resulting performances for all storms, with P_D and P_{FA} rates are presented in the last three rows. During ET-24h and ET+12h, our prediction analysis gives success rates of 60-70% according to the threshold chosen considering all storms. We wanted to compare the performance of the designed forecasting algorithm with that of NOGAPS. For this purpose, NOGAPS analysis and

prediction fields were generated for a time frame of 84 hours beginning at ET-24h. Then the same criterion explained in Section 2 was used to classify the storms according to NOGAPS. The numerical prediction system NOGAPS predicts 85% of these test storms correctly ($P_{FA} = 18\%$ and $P_D = 87\%$) at ET-24h where predictions of 84 hours ahead are considered, last column of Table 1. Table 1 also shows that storms 4, 6, 9, 11 and 18 consistently give True predictions. However, storms 1 and 14 are almost always predicted falsely. A more detailed investigation of the test storms together with possible reasons is presented in a future paper that discusses the meteorological aspects of the process.

Each of the storm observations has been projected onto a one-dimensional direction in an effort to reduce the dimensionality of the data in a way that maximizes separability of the two populations. Because the forecast decision is based on that projection distance, it is worthwhile understanding what the projection distance corresponds to physically, and how it helps our predictions. Therefore, we have constructed the two storm observations that correspond to the rightmost and leftmost end of the projection distance and present them at ET time in Figure 8. These correspond to our most negative (Figure 8(a)), our mean (Figure 8(b)), and most positive (Figure 8(c)) storm observations, as indicated by the asterisks on the line in Figure 4. Several features are evident that separate the negative storm observation from the positive storm observation at this time. These include more significant ridging ahead of the positive transitioning storm in Figure 8(c) compared with Figure 8(a), and a deeper embedding of the positive storm remnants in the baroclinic zone. There is a stronger zonal flow ahead of the negative storm in Figure 8(a) compared even with the mean image (Figure 8(b)) and the storm remnants exist as an open wave ahead of the trough compared with the mean image. These features correspond to some of those identified in studies of ET storms (Ritchie and Elsberry (2005), Harr et al. (2000)), and thus reflect that the algorithm is basing its prediction on real physical patterns.

5. Spatiotemporal Analysis

It was indicated in Section 3 that the separation distance between the two sets of storms increases consistently between ET-24h and ET+12h. The difference between the two distributions was utilized at discrete times to produce the forecasts presented in Section 4. However, the information we obtain from the discrete times can be combined to produce

a forecasting tool that incorporates the change in patterns with time. We designed two different methods to incorporate the sequence of events into the analysis to transform the spatial problem into a spatiotemporal one.

5a. Coupled Pattern Analysis

The first of the methods which we used to improve the spatial results is Coupled Pattern Analysis. We apply the Singular Value Decomposition (SVD) which has previously been used by Bretherton et al. (1992) to isolate coupled modes of variability between time series of two fields. The details of the application are described at the end of the paper in Section A. Spatial analysis used only one variable and EOF analysis used the covariance matrix for the corresponding analyses fields. The covariance matrix in spatial analysis can be represented by either HH^T or VV^T matrices in Figure 9 and these were used separately. Though, two different fields with possibly different dimensions can be used to find the coupled patterns and the matrices VH^T or HV^T could be used to find the variabilities between the classes. We take 500-mb geopotential height analysis from two consecutive times (ET-12h and ET+00h, etc.) and regard them as two different variables to utilize the information VH^T or HV^T may include.

The corresponding results of 27 storms from the years 2003-2004 are presented in the fifth, sixth and seventh columns of Table 1. These columns refer to the spatiotemporal results of ET-24h/ET-12h, ET-12h/ET+00h and ET+00h/ET+12h, respectively. The results indicate that coupled pattern analysis performs better than only spatial analysis at most of the chosen false alarm rates (Table 1).

5b. Combining the observations, "simple spatiotemporal analysis"

In the second of these methods, the new observations are composed of 500-mb geopotential height anomalies of each storm at two consecutive times, t_1 and t_2 . The same analysis steps in Figure 3 are then applied to the new anomaly field. The forecasting results for the 27 storms from the years 2003-2004 are presented in the eighth, ninth and tenth columns of Table 1. These columns refer to the spatiotemporal results of ET-24h/ET-12h, ET-12h/ET+00h and ET+00h/ET+12h, respectively. It can be concluded that the spatiotemporal results outperform the individual time results presenting higher detection and lower false alarm rates in almost all cases. This can better be confirmed comparing the correspond-

ing cells of ET-12h (spatial) to those of ET-24h/ET-12h (spatiotemporal), or ET+00h to ET-12h/ET+00h, etc. This is indeed an improvement of the more recent time, t_2 , results incorporating the data observation at time t_1 . Moreover, the performances in the last three rows indicate that coupled pattern analysis with SVD is not as effective as the simple spatiotemporal analysis. This could be because of the excessive coupling between the 500-mb geopotential height data coming from two consecutive times. Though our initial findings for the multivariable analysis indicate that coupled pattern analysis outperforms the separate variable analysis when two variables, 500-mb and vorticity, are used.

6. Future Work and Conclusion

A multi-stage projection pursuit technique is applied to NOGAPS 500-mb geopotential height analyses at different times to create a forecasting tool that predicts the outcome of various ET cases. The performance achieved on test data is less accurate than that of NOGAPS with a higher P_{FA} for the same detection performance, but the results are promising considering the fact that only one variable has been utilized, as opposed to NOGAPS, which includes full physical parameterizations. In addition, NOGAPS is computationally complex, and the algorithm proposed is a simpler approach.

Incorporating the change with time into the technique in two different ways using spatiotemporal analysis improved the results considerably. Initial results are promising and seem to be good starting point for future work.

In the future, we plan to automate the user-identified parts of the algorithm such as determining the ET+00h time. Moreover classification will be based on multiple classes rather than just two in a higher dimensional space. Utilization of other variables such as upper-level divergence (using the variable wind), remotely sensed optical and microwave data, will be investigated to improve the results as these variables provide differentiation between positive and negative storms. Addition of more variables will increase the computational complexity and new methods may be needed to execute the processing. We also plan to use forecast fields at earlier times to test the performance.

Acknowledgement I want to present my deepest thanks to my advisors Prof. Liz Ritchie and Prof. Scott Tyo. This paper would not have been possible without their strong support and recommendations.

References

- Bretherton, C. S., C. Smith, and J. M. Wallace, 1992: An intercomparison of methods for finding coupled patterns in climate data. *Journal of Climate*, **5**, 541–560.
- Demirci, O., E. A. Ritchie, and J. S. Tyo, 2004: Application of spatiotemporal pattern recognition techniques on predicting extratropical transition (and reintensification) of tropical cyclones. *Geoscience and Remote Sensing Symposium, 2004. IGARSS '04. Proceedings. 2004 IEEE International*, **1**, 452–455.
- Demirci, O., J. S. Tyo, and E. A. Ritchie, 2006: Spatial and spatiotemporal projection pursuit techniques to predict the extratropical transition of tropical cyclones. *submitted to the Transactions on Geoscience and Remote Sensing*.
- Harr, P. A., R. L. Elsberry, and T. F. Hogan, 2000: Extratropical transition of tropical cyclones over the western north pacific. part ii: The impact of midlatitude circulation characteristics. *Monthly Weather Review*, **128**, 2634–2653.
- Huber, P. J., 1985: Projection pursuit. *Annals of Statistics*, **13**, 435–475.
- Jones, S. C., P. A. Harr, J. Abraham, L. F. Bosart, P. J. Bowyer, J. L. Evans, D. E. Hanley, B. N. Hanstrum, R. E. Hart, F. Lalaurette, M. R. Sinclair, R. K. Smith, and C. Thorncroft, 2003: The extratropical transition of tropical cyclones: Forecast challenges, current understanding, and future directions. *Weather and Forecasting*, **18**, 1052–1092.
- Klein, P. M., P. A. Harr, and R. L. Elsberry, 2000: Extratropical transition of western north pacific tropical cyclones: An overview and conceptual model of the transformation stage. *Weather and Forecasting*, **15**, 373–396.
- Leuliette, E. W. and J. M. Wahr, 1999: Coupled pattern analysis of sea surface temperature and topex/poseidon sea surface height. *Journal of Physical Oceanography*, **29**, 599–611.
- Poor, H. V., 1994: *An Introduction to Signal Detection and Estimation*. Springer, New York.
- Ritchie, E. A. and R. L. Elsberry, 2005: Simulations of the extratropical transition of tropical cyclones: phasing between the upper-level trough and tropical cyclone. *submitted to Monthly Weather Review*.

Wallace, J. M., C. Smith, and C. S. Bretherton, 1992: Singular value decomposition of wintertime sea surface temperature and 500-mb height anomalies. *Journal of Climate*, **5**, 561–576.

A. Application of SVD

Two variable fields do not necessarily have to have the same dimensions. Another anomaly matrix Y can be obtained using the $(k \times l)$ dimensional data images for each storm. These variables can be arranged into a $(kl \times N)$ data matrix, Y . The $(kl \times mn)$ dimensional cross correlation matrix of the two variables can be defined as,

$$\hat{C}_{yx} = \frac{1}{N-1} Y X^T. \quad (1)$$

Singular value decomposition of the cross correlation matrix is

$$\hat{C}_{yx} = U_{(kl \times kl)} S_{(kl \times mn)} V_{(mn \times mn)}^T, \quad (2)$$

where columns of U , \mathbf{u}_k , are called as left singular vectors and columns of V , \mathbf{v}_k , are called as right singular vectors. These columns are orthogonal to each other, $U^T U = I$ and $V V^T = I$. \mathbf{u}_k 's and \mathbf{v}_k 's are eigenvectors of $\hat{C}_{yx} \hat{C}_{yx}^T$, and $\hat{C}_{yx}^T \hat{C}_{yx}$, respectively. r singular values in $S_{(kl \times mn)}$ are square roots of nonzero eigenvalues of both $\hat{C}_{yx} \hat{C}_{yx}^T$, and $\hat{C}_{yx}^T \hat{C}_{yx}$.

Instead of using two different variables, SVD analysis can be used on the same variable but at different times. In this case, cross correlation matrix is defined as,

$$\hat{C}_{x_{t_1} x_{t_2}} = \frac{1}{N-1} X_{t_1} X_{t_2}^T. \quad (3)$$

In our study, we are utilizing the cross correlation information of 500-mb geopotential height data at different times. Observation vectors are projected onto the left and right singular vectors and storm observations can be represented in a lower dimensional space similarly,

$$P' = V^T X_{t_1} + U^T X_{t_2}. \quad (4)$$